



Giuggioli, L., Gupta, S., & Chase, M. (2019). Comparison of two models of tethered motion. *Journal of Physics A: Mathematical and Theoretical*, 52(7), [075001]. <https://doi.org/10.1088/1751-8121/aaf8cc>

Peer reviewed version

License (if available):
CC BY-NC-ND

Link to published version (if available):
[10.1088/1751-8121/aaf8cc](https://doi.org/10.1088/1751-8121/aaf8cc)

[Link to publication record in Explore Bristol Research](#)
PDF-document

This is the author accepted manuscript (AAM). The final published version (version of record) is available online via IOP at <https://iopscience.iop.org/article/10.1088/1751-8121/aaf8cc/meta> . Please refer to any applicable terms of use of the publisher.

University of Bristol - Explore Bristol Research

General rights

This document is made available in accordance with publisher policies. Please cite only the published version using the reference above. Full terms of use are available:
<http://www.bristol.ac.uk/red/research-policy/pure/user-guides/ebr-terms/>

Comparison of two models of tethered motion

Luca Giuggioli^{1,2}, Shamik Gupta³, Matt Chase⁴

¹Bristol Centre for Complexity Sciences, University of Bristol, Bristol, UK

²Department of Engineering Mathematics, University of Bristol, Bristol, UK

³Department of Physics, Ramakrishna Mission Vivekananda University, Belur Math, Howrah 711202, India

⁴Department of Physics and Astronomy, University of New Mexico, Albuquerque, NM, USA

E-mail: Luca.Giuggioli@bristol.ac.uk

Abstract. We consider a random walker whose motion is tethered around a focal point. We use two models that exhibit the same spatial dependence in the steady state but widely different dynamics. In one case, the walker is subject to a deterministic bias towards the focal point, while in the other case, it resets its position to the focal point at random times. The deterministic tendency of the biased walker makes the forays away from the focal point more unlikely when compared to the random nature of the returns of the resetting walker. This difference has consequences on the spatio-temporal dynamics at intermediate times. To show the differences in the two models, we analyze their probability distribution and their dynamics in presence and absence of partially or fully absorbing traps. We derive analytically various quantities: (i) mean first-passage times to one target, where we recover results obtained earlier by a different technique, (ii) splitting probabilities to either of two targets as well as survival probabilities when one or either target is partially absorbing. The interplay between confinement, diffusion and absorbing traps produces interesting non-monotonic effects in various quantities, all potentially accessible in experiments. The formalism developed here may have a diverse range of applications, from study of animals roaming within home ranges and of electronic excitations moving in organic crystals to developing efficient search algorithms for locating targets in a crowded environment.

PACS numbers:

Keywords:

1. Introduction

Tethered motion has relevance in a variety of context and represents the inability of a particle or agent to stray afar from a given location in space, the so-called focal point. Animals that keep returning to their burrow for shelter or for caching resources, or animals who do not have a den but who move away from predators or other conspecifics and tend to return to the same area are ecological examples [1]. Other worthwhile

examples to cite are searchers that reset their position to their initial starting place after being unsuccessful for some time [2], or a cell population that suffers an abrupt event and its density gets reduced to some specified lower value, e.g., tumors after chemical treatment [3].

Although in all the above cases, the steady-state probability is expected to be localized around a focal point or value, the difference between the first and the last two examples cited above is that an agent moves towards the focal point by going through the intervening space in the first case, whereas it does not do so in the last two cases. This difference has two important consequences. Firstly, the formalism for analytically characterizing the former is a Smoluchowski-type diffusion equation, while that for the latter is the diffusion equation with stochastic resetting [4]. Secondly, the steady-state probability distribution for the animal example is an equilibrium state, while it is not so for the resetting case where detailed balance does not hold [5].

Analysis of the resetting example has shown that the steady-state probability distribution is an exponential symmetric around the focal point [4, 6]. As the spatial dependence in the steady state of the Smoluchowski-type diffusion equation depends on the deterministic tendency towards the focal point, we choose for comparison a model where the steady state is also a symmetric exponential, which corresponds to a motion subject to a constant bias towards the focal point.

As the spatial distribution at long times for the two models coincides, the fundamental difference of the two processes should clearly appear in the dynamics. Here we are interested in unraveling such differences by comparing the models in one dimension (1D). For comparison, we discuss the form of the propagators and some of their moments, and also discuss applications to two reaction-diffusion scenarios.

The paper is laid out as follows. In Sec. 2, we describe the two tethered models that we will use for comparison. We name drift model the case where the motion is subject to a constant deterministic bias towards the focal point, to distinguish it from the (sudden) resetting model. We will present exact analytical expressions for the spatial distribution, and analyze in detail the time dependence of the mean and the mean-squared displacement from the focal point. Section 3 is dedicated to the formalism to treat the case in which the motion takes place in presence of a trap. We also show how to compute the yield, that is, the number of particles getting absorbed at a detector placed at the trap location, when the motion represents the movement of a particle decaying over time. In Sec. 4, we study in all three cases the parameter dependence of the mean first-passage time to a given target. In Sec. 5, we consider the scenario of two targets, construct the probability distribution and investigate aspects related to the splitting probability, namely, the probability of reaching one of the targets (without having been at the other) as a function of the initial distance from it. Finally, Sec. 6 constitutes the concluding section.

2. Focal point models

The common characteristic of the two models is that the uncertainty in the movement of the stochastic observable through space is represented by Brownian diffusion. We may therefore refer to the stochastic variable as representing the state of a random walker. The tendency or the bias to move towards the focal point on the other hand distinguishes the two models qualitatively. In the case of the drift model, the bias is represented by a constant drift towards the focal point that is present *at all times*, while in the case of the stochastic resetting model, the bias is represented through a long jump (an infinitely fast movement) to the focal point *at random times*. The former is an example of a Smoluchowski-type model that has been used in various contexts, e.g., to model Brownian particles subject to dry friction [7] and motion of excitons in doped molecular crystals and signal receptor clusters on the surface of T-cells during immunological synapse formation [8]. It has also appeared in the animal movement literature to represent movement within a home range, and is called the Holgate-Okubo model [9, 10, 11]. The stochastic resetting model was introduced more recently to model search processes in a crowded environment [4].

In the following, we consider the motion of the walker to be taking place in one dimension. We take (x, t) to represent space and time, respectively, and consider the constant $D > 0$ to represent the diffusion constant, x_0 to represent the initial location of the walker and x_c to denote the focal point to which the motion of the walker is biased. In the constant drift model, the position of the walker evolves in time according to the Langevin equation of motion

$$\frac{dx}{dt} = -\frac{\partial V(x)}{\partial x} + \sqrt{2D} \eta(t), \quad (1)$$

where $\eta(t)$ is a Gaussian, white noise with zero mean and with correlation given by

$$\langle \eta(t)\eta(t') \rangle = \delta(t - t'). \quad (2)$$

Here and in the following, angular brackets denote averaging over noise realizations. We take the potential $V(x)$ to be of the form $V(x) = v|x - x_c|$, where the parameter v represents a speed. In the stochastic resetting model, while at position x at time t , the walker in the ensuing infinitesimal time interval dt has the following choices for updating its location:

$$\text{With probability } 1 - rdt, \text{ following the dynamics } \frac{dx}{dt} = \sqrt{2D} \eta(t), \quad (3)$$

$$\text{With probability } rdt, \text{ resetting to the focal point } x_c. \quad (4)$$

Here, $r \geq 0$ is a parameter that characterizes the rate of resetting, that is, the probability to reset per unit time. The dynamics of the resetting model involves indeed a restart or a “reset” of the motion from x_c at random times, where x_c may be viewed as the reset location. From the foregoing, it follows that the time interval τ between successive resets is a random variable distributed according to an exponential distribution $\rho(\tau) = re^{-r\tau}$.

To provide a demonstration of the difference between the two models, we plot in Fig. 1 two typical trajectories, one for the constant drift model and one for the resetting model.

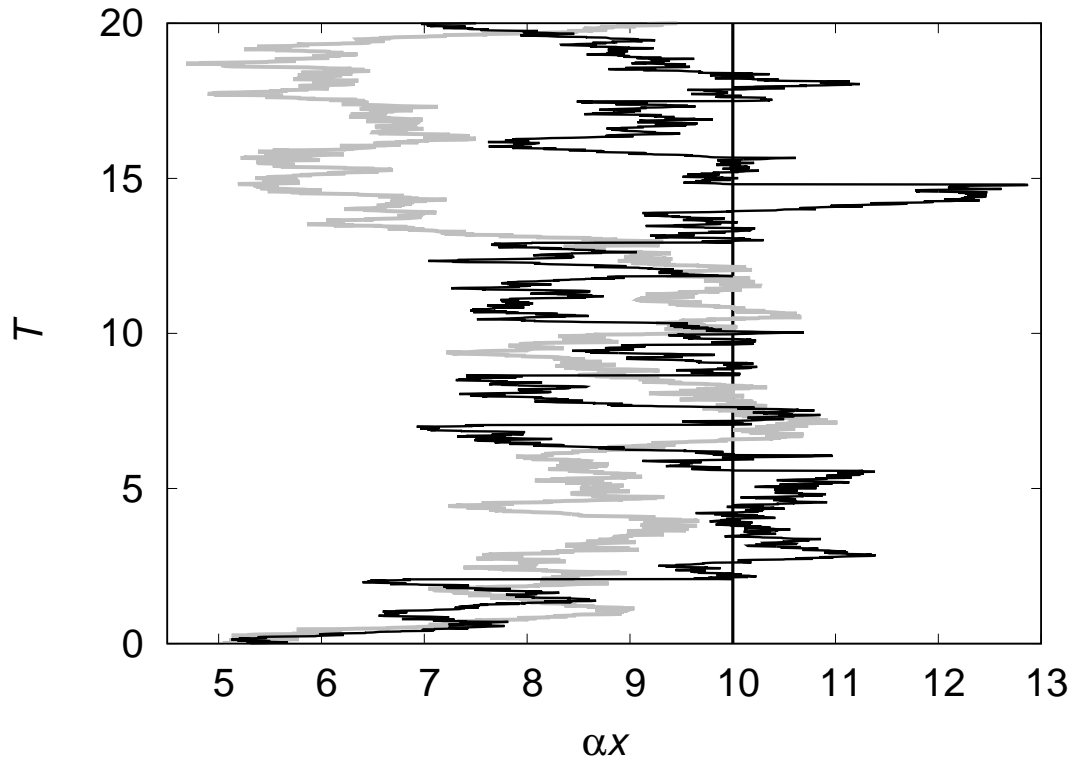


Figure 1. Representative trajectories for the constant drift model and the stochastic resetting model. The black trajectory refers to stochastic resetting model, while the grey one corresponds to the drift model. The values of the dynamical parameters of the two models are chosen so as to have the steady-state characteristic spatial scale in the two models the same, by setting $v/D = \sqrt{r/D} = \alpha$, see Eqs. (8) and (13). The temporal scale is on the other hand set to $rt = T$ for the drift model and $v^2t/D = T$ for the resetting model. Here, we take $\alpha x_0 = 5$ and $\alpha x_c = 10$, with the latter indicated in the plot with a vertical line. Notice the presence of horizontal segments in the black trajectory corresponding to time instants when the walker resets to x_c , which are instead lacking in the grey trajectory for the constant drift model.

2.1. The drift model

The probability distribution $P(x, t|x_0, 0)$ to find the walker at position x at time t , given that it was at x_0 at time $t = 0$, that is $P(x, 0) = \delta(x - x_0)$, where $\delta(z)$ represents a Dirac delta, is governed by the Fokker-Planck (FP) equation

$$\frac{\partial P(x, t)}{\partial t} = v \frac{\partial}{\partial x} \left[\frac{x - x_c}{|x - x_c|} P(x, t) \right] + D \frac{\partial^2 P(x, t)}{\partial x^2}. \quad (5)$$

Exact solution of Eq. (5) for any x and x_0 can be found in two ways. A separation of variable allows to map the problem to an eigenvalue problem of the Sturm-Liouville

type [7]. Another way is to solve the equation in the Laplace variable ϵ , that is, to find $\tilde{P}(x, \epsilon|x_0, 0) \equiv \int_0^\infty dt e^{-\epsilon t} P(x, t|x_0, 0)$ in the region to the left and to the right of x_0 , and then match the two solutions at x_0 to obtain [8]

$$\tilde{P}(x, \epsilon|x_0, 0) = \frac{e^{-\frac{v(|x-x_c|-|x_0-x_c|)}{2D}}}{v\sqrt{1+\frac{4D\epsilon}{v^2}}} \left[e^{-\frac{v|x-x_0|\sqrt{1+4D\epsilon/v^2}}{2D}} + \frac{e^{-\frac{v(|x-x_c|+|x_0-x_c|)\sqrt{1+4D\epsilon/v^2}}{2D}}}{\sqrt{1+\frac{4D\epsilon}{v^2}} - 1} \right]. \quad (6)$$

Inverse Laplace transform of the above expression then yields [8]

$$P(x, t|x_0, 0) = \frac{1}{\sqrt{4\pi Dt}} e^{-\frac{(x-x_0)^2}{4Dt}} e^{-\frac{v^2 t}{4D}} e^{-\frac{v(|x-x_c|-|x_0-x_c|)}{2D}} + \frac{ve^{-\frac{v|x-x_c|}{D}}}{4D} \left[1 - \text{Erf} \left(\frac{|x-x_c|+|x_0-x_c|-vt}{\sqrt{4Dt}} \right) \right], \quad (7)$$

with $\text{Erf}(x) = (2\pi)^{-1} \int_0^x ds e^{-s^2}$ being the error function. In the limit $t \rightarrow +\infty$, Eq. (7) yields the steady state distribution

$$P_{\text{ss}}(x) = \frac{v}{2D} e^{-v|x-x_c|/D}. \quad (8)$$

From Eq. (7), we obtain the mean position as

$$\langle x - x_0 \rangle(t) = x_c - x_0 + \frac{vt - (x_c - x_0)}{2} \text{Erfc} \left[\frac{1}{2} \left(\sqrt{\frac{t}{D}} v - \frac{x_c - x_0}{\sqrt{Dt}} \right) \right] e^{\frac{v[|x_c-x_0|-(x_c-x_0)]}{2D}} - \frac{vt + (x_c - x_0)}{2} \text{Erfc} \left[\frac{1}{2} \left(\sqrt{\frac{t}{D}} v + \frac{x_c - x_0}{\sqrt{Dt}} \right) \right] e^{\frac{v[|x_c-x_0|+(x_c-x_0)]}{2D}}, \quad (9)$$

where $\text{Erfc}(x) \equiv 1 - \text{Erf}(x)$ is the complementary error function. Equation (9) is identically zero for $x_0 = x_c$, is non-zero for any finite t if $x_0 \neq x_c$, and equals $x_c - x_0$ at long times. The calculation of the mean-squared displacement (MSD) is more involved, but can be done analytically. While we have reported the full general expression in Appendix A, for the simple case of $x_0 = x_c$, we have

$$\langle (x-x_c)^2 \rangle(t) = 2\frac{D^2}{v^2} - \left[\sqrt{\frac{Dt}{\pi}} \left(vt + 2\frac{D}{v} \right) \right] e^{-\frac{v^2 t}{4D}} + \left(2Dt + \frac{v^2 t^2}{2} - 2\frac{D^2}{v^2} \right) \text{Erfc} \left(\frac{1}{2} \sqrt{\frac{t}{D}} v \right). \quad (10)$$

While in the general case, i.e., for $x_0 \neq x_c$, the short time dependence of the MSD is $2Dt + v^2 t^2$, which is the expected time dependence of a diffusing particle subject to a drift, this is not the case for $x_0 = x_c$. At short times, in fact, Eq. (10) increases proportionally to $2Dt - \frac{8}{3} \sqrt{\frac{v^2 Dt^3}{\pi}} + \frac{v^2 t^2}{2}$. This is because when a walker starts at the centre, the potential acts to confine the walker around the origin rather than forcing it towards x_c . As the walker diffuses outward, the potential should reduce the MSD depending on its strength v and the rate at which the walker diffuses that depends on D . This is why the expected drift $v^2 t^2$ is reduced by a factor two and the additional contribution proportional to $t^{3/2}$ is negative.

2.2. The stochastic resetting model

We now discuss the model of stochastic resetting. Recognizing that at each reset, the motion starts afresh (gets “renewed”) at x_c , we may straightforwardly obtain the probability $P(x, t|x_0, 0)$. At a fixed time t , let the time elapsed since the last renewal be in $[\tau, \tau + d\tau]$, with $0 \leq \tau \leq t$. Noting that the probability for this event is $r \exp(-r\tau)d\tau$, we have

$$P(x, t|x_0, 0) = \int_0^t d\tau r \exp(-r\tau) P_d(x, t|x_c, t - \tau) + \exp(-rt) P_d(x, t|x_0, 0), \quad (11)$$

where $P_d(x, t|x_c, t - \tau) \equiv e^{-(x-x_c)^2/(4D\tau)}/\sqrt{4\pi D\tau}$ is the propagator of free diffusion. Integrating Eq. (11) over $x \in [-\infty, \infty]$, and using the normalization $\int_{-\infty}^{\infty} dx P_d(x, t|x_0, t') = 1 \forall x_0$ and for $t > t'$, it may be checked that $P(x, t|x_0, 0)$ is correctly normalized to unity. From Eq. (11), we obtain

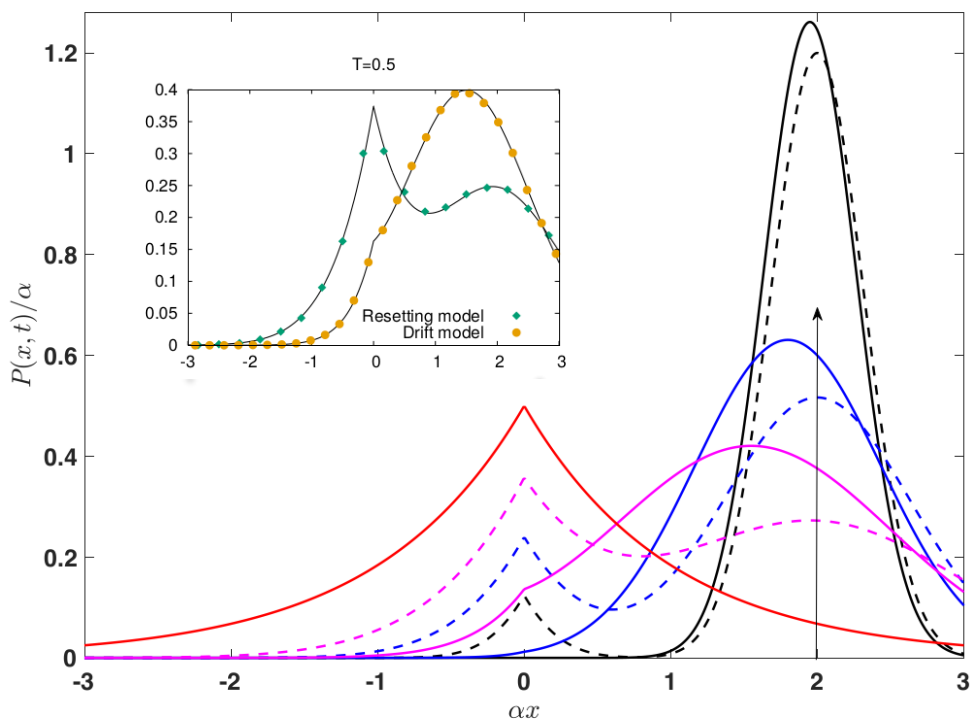


Figure 2. (Color online) Comparison of the time-dependent probability distribution for the drift model (solid line) in Eq. (7), and the resetting model (dashed line) in Eq. (12). The arrow corresponds to the localized initial position at $\alpha x_0 = 2$, while the focal point is set at $\alpha x_c = 0$. The solid curve symmetric around the origin is the steady state distribution, identical for both models, while the other curves, starting from the highest curves on the right, represent the two models at times $T=0.05, 0.45$, and 9.95 . The inset shows the match between theory and simulations for $T = 0.5$. The parameter α and the rescaled time T are the same as in Fig. 1.

$$P_{\text{reset}}(x, t|x_0, 0) = \frac{e^{-rt - \frac{(x-x_0)^2}{4Dt}}}{\sqrt{4\pi Dt}} + \frac{1}{4}\sqrt{\frac{r}{D}}e^{-\sqrt{\frac{r}{D}}|x-x_c|}\text{Erfc}\left(\frac{|x-x_c|}{2\sqrt{Dt}} - \sqrt{rt}\right) - \frac{1}{4}\sqrt{\frac{r}{D}}e^{\sqrt{\frac{r}{D}}|x-x_c|}\text{Erfc}\left(\frac{|x-x_c|}{2\sqrt{Dt}} + \sqrt{rt}\right), \quad (12)$$

whose steady-state form is

$$P_{\text{ss}}(x) = \frac{1}{2}\sqrt{\frac{r}{D}}e^{-|x-x_c|\sqrt{r/D}}. \quad (13)$$

As expected, the steady-state distribution does not depend on the initial location x_0 . For the particular case when the initial location x_0 is the same as the reset location x_c , Eq. (13) reduces to the result obtained in Ref. [4].

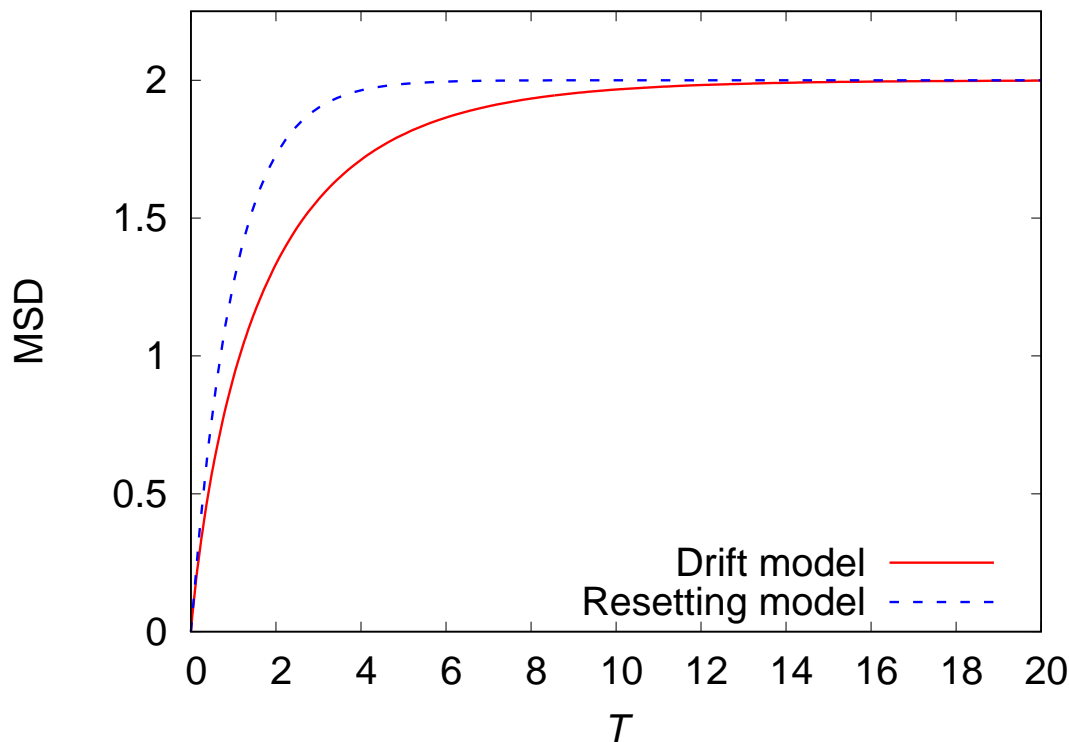


Figure 3. (Color online) MSD in the drift model and the resetting model, given respectively by Eqs. (10) and (17) with $x_c = x_0$, as a function of the dimensionless time T . We used $\alpha = 1$ for both models.

Corresponding to the distribution (12), the mean displacement from the initial location is given by

$$\langle(x-x_0)\rangle(t) = \langle(x-x_0)\rangle'(t), \quad (14)$$

where the prime denotes averaging with respect to the second and the third term on the right hand side (rhs) of Eq. (12), and we have used the fact that when averaged with respect to the first term, the mean displacement from the initial location evaluates to zero. Next, we rewrite the rhs of Eq. (14) to obtain

$$\langle(x-x_0)\rangle(t) = \langle(x-x_c)\rangle'(t) + (x_c - x_0)\langle 1 \rangle'(t) = (x_c - x_0)(1 - e^{-rt}), \quad (15)$$

where in obtaining the last equality, we have used the fact that $\langle(x - x_c)\rangle'(t) = 0$ because of the symmetry of the second and the third term on the rhs of Eq. (12) under $x \rightarrow -x, x_c \rightarrow -x_c$, and that $\langle 1 \rangle' = 1 - e^{-rt}$

Similarly, one may compute the MSD as a function of time:

$$\langle(x - x_0)^2\rangle(t) = \langle(x - x_c)^2\rangle'(t) + (x_c - x_0)^2\langle 1 \rangle'(t) + 2(x_c - x_0)\langle(x - x_c)\rangle'(t) + 2Dte^{-rt}, \quad (16)$$

where the fourth term on the right is the result obtained by averaging with respect to the first term on the rhs of Eq. (12). We finally get

$$\begin{aligned} \langle(x - x_0)^2\rangle(t) &= \frac{2D}{r} [1 - e^{-rt}(1 + rt)] + (x_c - x_0)^2(1 - e^{-rt}) + 2Dte^{-rt} \\ &= \left[\frac{2D}{r} + (x_c - x_0)^2 \right] (1 - e^{-rt}). \end{aligned} \quad (17)$$

To find the ϵ expression for the propagator, it is straightforward to Laplace transform Eq. (11), rather than Eq. (12), to obtain

$$\tilde{P}(x, \epsilon | x_0, 0) = \frac{e^{-|x-x_0|\sqrt{(r+\epsilon)/D}}}{2\sqrt{D(r+\epsilon)}} + \frac{r e^{-|x-x_c|\sqrt{(r+\epsilon)/D}}}{\epsilon 2\sqrt{D(r+\epsilon)}}. \quad (18)$$

For convenience that will become evident in Sec. 5, it is better to have the following compact expression for the Laplace propagators:

$$\tilde{P}(x, \epsilon | x_0, 0) = h_{x_c}(x, x_0) \frac{\mathcal{C}(\epsilon)e^{-\alpha|x-x_0|\mathcal{S}(\epsilon)} + \mathcal{D}_{x_c}(x_0, \epsilon)e^{-\alpha|x-x_c|\mathcal{S}(\epsilon)}}{2\mathcal{C}(\epsilon)\mathcal{S}(\epsilon)}, \quad (19)$$

with

$$\begin{aligned} \alpha &= \frac{v}{D}, & h_{x_c}(y, z) &= \frac{e^{-\alpha(|y-x_c|-|z-x_c|)/2}}{v}, & \mathcal{D}_{x_c}(y, \epsilon) &= e^{-\alpha|y-x_c|\mathcal{S}(\epsilon)}, \\ \mathcal{S}(\epsilon) &= \frac{\sqrt{1 + \frac{4D\epsilon}{v^2}}}{2}, & \mathcal{C}(\epsilon) &= 2\mathcal{S}(\epsilon) - 1, \end{aligned} \quad (20)$$

for the drift model, and with

$$\alpha = \sqrt{\frac{r}{D}}, \quad h_{x_c}(y, z) = \frac{1}{\sqrt{Dr}}, \quad \mathcal{D}_{x_c}(y, \epsilon) = 1, \quad \mathcal{S}(\epsilon) = \sqrt{1 + \frac{\epsilon}{r}}, \quad \mathcal{C}(\epsilon) = \frac{\epsilon}{r}, \quad (21)$$

for the resetting model.

A comparison of the dynamics of the probability distribution of the two models in Fig. 2 shows how in the resetting model the random walker moves through the intervening space so that the probability distribution at short times remains close to zero in the space between the origin and the initial position x_0 . From Fig. 2, it is also evident that far from the initial position x_0 , the probability distribution for the drift model is always smaller than the corresponding one for the reset model. The limited dispersion of the drifting versus the resetting walker is more clearly visible when the initial location is $x_0 = x_c$. In such a case, it is sufficient to plot the MSD and notice that its value for the reset model is always larger than that for the drift model (see Fig. 3).

3. Traps, impartial detection and yield

In many scenarios, the walker dynamics may be subject to physical constraints. When certain locations in the space the walker is roaming about hinder the movement, the landscape may be represented by partially absorbing traps that capture the walker for some time [12]. The walker may also represent a searcher seeking a target that is partially hidden, and so the capture of that target may not occur upon reaching the target for the first time but only after a larger number of encounters. In this case, one is interested in estimating the probability of capture as a function of time. In both these cases, the walker may undergo, in addition, a decay before the absorption at the trap is complete or before the target is detected, e.g., a diffusing molecular excitation with a radiative decay in presence of a trap with imperfect capture [13] or an animal being predated while foraging [14]. To help interpret each parameter of the system when one is using either of the two models in the context of a forager/searcher or an electronic excitation, we have created Table 3.

	C	v	r	τ
electronic excitation	absorption rate of detector	strength attracting centre	reset rate to attracting centre	excitation decay rate
foraging animal	detection rate of concealed food items	movement bias to home range centre	jump return rate to home range centre	predation rate

Table 1. Interpretation of the different model parameters depending on system being modelled in Eq. (22) and (23).

To account for the aforementioned dynamical scenarios, it is necessary to augment the equation for the spatial probability distribution with two additional terms: a probability loss with a decay rate τ^{-1} and a rate of absorption C (per unit distance) at the traps, or, a rate C of imperfect detection of the target. For the simple case of one trap or target located at x' , we have

$$\frac{\partial \mathcal{P}(x, t)}{\partial t} + \frac{\mathcal{P}(x, t)}{\tau} = v \frac{\partial}{\partial x} \left[\frac{x - x_c}{|x - x_c|} \mathcal{P}(x, t) \right] + D \frac{\partial^2 \mathcal{P}(x, t)}{\partial x^2} - C \delta(x - x') \mathcal{P}(x, t), \quad (22)$$

with the initial condition $P(x, 0) = \delta(x - x_0)$ for the constant drift model, and

$$\mathcal{P}(x, t|x_0, 0) = e^{-\frac{t}{\tau}} P(x, t|x_0, 0) - C \int_0^t ds e^{-\frac{t-s}{\tau}} P(x, t-s|x', 0) \mathcal{P}(x', s|x_0, 0) \quad (23)$$

for the resetting model. While the former equation follows the standard literature [15], the latter is being reported here for the first time. In Eq. (23) the first term contains the defect-free propagator $P(x, t|x_0, 0)$, given by Eq. (12), multiplied by $\exp(-t/\tau)$ to represent the loss of probability irrespective of the spatial position. The second term indicates instead that there is a loss of probability with rate C if the walker was at x' at some earlier time s , which is a term proportional to the probability $\mathcal{P}(x', s|x_0, 0)$. As the equation describes the probability of being at x as a function of time t , $\mathcal{P}(x', s|x_0, 0)$ is

multiplied with the probability of moving from x' to x in the interval $t - s$, that is, with $e^{-(t-s)/\tau} P(x, t - s | x', 0)$. As the probability loss due to the walker being at x' may occur at any earlier time s , the term $e^{-(t-s)/\tau} P(x, t - s | x', 0) \mathcal{P}(x', s | x_0, 0)$ is then integrated over all times s .

Given the linearity of Eqs. (22) and (23) the exact solution in Laplace domain can be obtained by application of the so-called defect technique [16, 17], which allows to write the propagator $\mathcal{P}(x, t | x_0, 0)$ of the defect problem in terms of the defect-free propagator $P(x, t | x_0, 0)$. By exploiting the linearity in probability space and realizing that the second term in Eqs. (22) and the exponential $\exp(-t/\tau)$ in Eq. (23) simply transform the functional form of the propagator (with defect) from being expressed in terms of ϵ to being expressed in terms of $\epsilon + 1/\tau$, one has for both models

$$\tilde{\mathcal{P}}(x, \epsilon | x_0, 0) = \tilde{P}(x, \epsilon + \tau^{-1} | x_0, 0) - \frac{\tilde{P}(x, \epsilon + \tau^{-1} | x', 0) \tilde{P}(x', \epsilon + \tau^{-1} | x_0, 0)}{\frac{1}{C} + \tilde{P}(x', \epsilon + \tau^{-1} | x', 0)}. \quad (24)$$

The terms on the rhs depend in both cases on the defect free propagator, which are given explicitly by Eqs. (19) and (20) for the drift model, and by Eqs. (19) and (21) for the resetting model.

We proceed by adopting quantum yield calculations [18, 19] that were used in the understanding of the motion of Frenkel excitons in doped molecular crystals [20, 21]. Electronic excitations, generated by light impulses, move through the material and are subject to either radiative decay or absorption by one of a small number of guest molecules introduced into the host crystal [22]. Though quantum mechanical in nature, the excitations were found to move incoherently on the lattice [15] due to the weak coupling between the organic crystals [20, 21]. The resulting equations that describe their dynamics are therefore for *probabilities*, and not for amplitudes, and are in the form given by

$$\frac{\partial \mathcal{P}_e(x, t)}{\partial t} + \frac{\mathcal{P}_e(x, t)}{\tau_e} = \{\text{Motion Terms}\} - C_e \delta(x - x_e) \mathcal{P}_e(x, t), \quad (25)$$

where $\{\text{Motion Terms}\}$ describes the motion of the excitation in the absence of the guest molecules and is generally diffusive [18, 15]. Effects of the radiative decay and capture are specified by the parameters τ_e , C_e , and x_e , which, respectively, represent the excitation decay time, the capture rate (per unit distance) and the location of the guest site.

The quantum yield provides a useful timescale with which to compare empirical findings. It is found by integrating $\mathcal{P}_e(x, t)$ over all space that

$$\tilde{\phi}(\epsilon) = \int_{-\infty}^{\infty} dx \tilde{\mathcal{P}}_e(x, \epsilon) \quad (26)$$

represents the ratio of the number of excitations that have been absorbed by a guest molecule and radiated from the host to those that were originally created in the host. Although the quantum yield is in general time dependent, its value integrated over all times, that is, $\tilde{\phi}(0)$, provides an effective rate that can be used in more complex models.

Though we do not propose that our formalism is necessarily applicable to the study of motion of excitations in doped molecular crystals, the quantum yield style calculations outlined above have found recent use in other systems. For example, in the context of Smoluchowski random walkers [23] and in the transmission of infectious epidemics [24], it was demonstrated that the interplay between diffusion, confinement and absorption at site x' may bring about non-monotonic dependencies of the quantum yield. We explore below such non-monotonic dependencies in our formalism.

With the addition of localized absorption and decay, Eq. (22) is transformed to

$$\begin{aligned} \frac{\partial \mathcal{P}_e(x, t)}{\partial t} + \frac{\mathcal{P}_e(x, t)}{\tau} + \frac{\mathcal{P}_e(x, t)}{\tau_e} = v \frac{\partial}{\partial x} \left[\frac{x - x_c}{|x - x_c|} \mathcal{P}_e(x, t) \right] \\ + D \frac{\partial^2 \mathcal{P}_e(x, t)}{\partial x^2} - C \delta(x - x') \mathcal{P}_e(x, t) - C_e \delta(x - x_e) \mathcal{P}_e(x, t). \end{aligned} \quad (27)$$

To take into account the additional presence of the absorption site as well as the

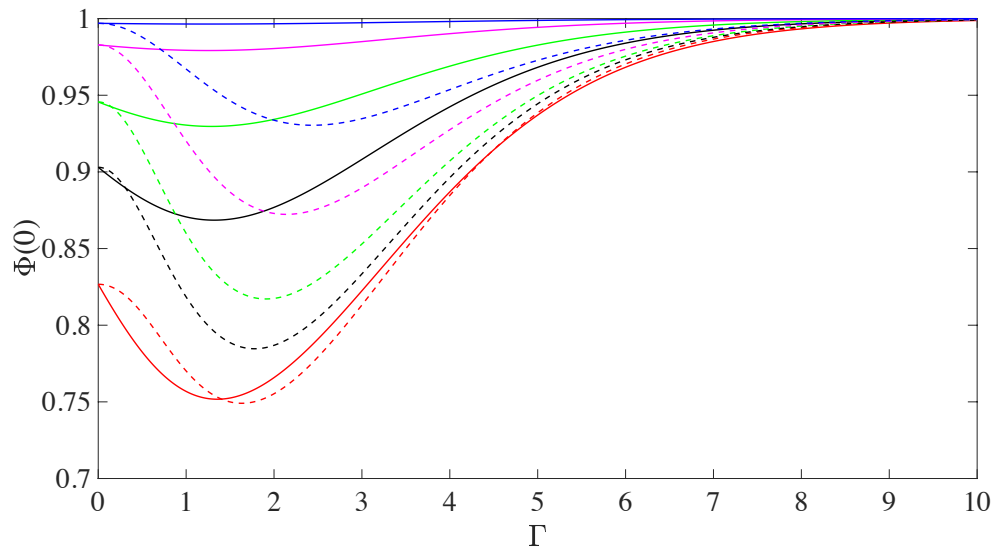


Figure 4. (Color online) Quantum yield as defined in Eq. (30) is plotted as a function of the strength of the confinement Γ . The vertical axis is made dimensionless by using $\Phi(0) = \tilde{\phi}(0)[\tau + \tau_e]/\tau\tau_e$. Every distance is expressed relative to the distance of the guest molecule to the focal point, i.e. $|x_e - x_c|$ and the strengths of the absorption at the trap and guest molecule are expressed through the dimensionless quantities $\mathcal{C} = C|x_e - x_c|/D$ and $\mathcal{C}_e = C_e|x_e - x_c|/D$, respectively. Starting from the bottom the dashed and solid curves, representing the reset and drift cases, respectively, are plotted with increasing values of R , namely $R = 0.75, 1, 1.25, 1.75$ and 2.5 . For all curves the trap and guest molecule absorption strength has been set equal with $\mathcal{C} = \mathcal{C}_e = 4$.

probability decay with rate τ_e the integral Eq. (23) is modified to

$$\begin{aligned} \mathcal{P}_e(x, t|x_0, 0) &= e^{-\left(\frac{1}{\tau} + \frac{1}{\tau_e}\right)t} P_{\text{reset}}(x, t|x_0, 0) \\ &\quad - C \int_0^t ds e^{-\left(\frac{1}{\tau} + \frac{1}{\tau_e}\right)(t-s)} P_{\text{reset}}(x, t-s|x', 0) \mathcal{P}_e(x', s|x_0, 0) \\ &\quad - C_e \int_0^t ds e^{-\left(\frac{1}{\tau} + \frac{1}{\tau_e}\right)(t-s)} P_{\text{reset}}(x, t-s|x', 0) \mathcal{P}_e(x', s|x_0, 0). \end{aligned} \quad (28)$$

Notice that both τ_e and C_e may in principle differ from their respective counterparts radiative decay τ of the exciton moving through the host.

Once again the defect technique allows us to solve for $\mathcal{P}_e(x, t)$ in Eq. (27) or (28). The problem is more complicated given that we are dealing with two defects rather than one, but the procedure is the same as for the one defect problem. As the solution of the defect-free problem with the addition of the loss term at rate $\mathcal{T}^{-1} = 1/\tau + 1/\tau_e$ is known, namely $\tilde{P}(x, \epsilon + \mathcal{T}^{-1}|x_0, 0)$, one can write the formal solution of Eq. (27) as

$$\begin{aligned} \tilde{\mathcal{P}}_e(x, \epsilon|x_0, 0) &= \tilde{P}(x, \epsilon + \mathcal{T}^{-1}|x_0, 0) - C\tilde{P}(x, \epsilon + \mathcal{T}^{-1}|x', 0) \tilde{\mathcal{P}}_e(x', \epsilon|x_0, 0) \\ &\quad - C_e\tilde{P}(x, \epsilon + \mathcal{T}^{-1}|x_e, 0) \tilde{\mathcal{P}}_e(x_e, \epsilon|x_0, 0). \end{aligned} \quad (29)$$

For Eq. (28) the solution is of the same form. It suffices to replace $\tilde{P}(y, s|z, 0)$ with $\tilde{P}_{\text{reset}}(y, s|z, 0)$.

To determine the general solution one needs to evaluate Eq. (29) at the point x' and x_e . One then finds $\tilde{\mathcal{P}}_e(x_e, \epsilon|x_0, 0)$ and $\tilde{\mathcal{P}}_e(x', \epsilon|x_0, 0)$ by solving two coupled algebraic equations. The result of the calculation gives the probability distribution and is shown in Appendix B. Using the explicit expression in Eq. (B2) it is now possible to calculate the ‘quantum yield’. For the drift model it is given by

$$\begin{aligned} \tilde{\phi}(0) &= \mathcal{T} \left(1 - \left\{ \left[1 + C_e \tilde{P}(x_e, \mathcal{T}^{-1}|x_e, 0) \right] C\tilde{P}(x', \mathcal{T}^{-1}|x_0, 0) - C_e \tilde{P}(x', \mathcal{T}^{-1}|x_e, 0) \right. \right. \\ &\quad \times C\tilde{P}(x_e, \mathcal{T}^{-1}|x_0, 0) + \left. \left[1 + C\tilde{P}(x', \mathcal{T}^{-1}|x', 0) \right] C_e \tilde{P}(x_e, \mathcal{T}^{-1}|x_0, 0) - C\tilde{P}(x_e, \mathcal{T}^{-1}|x', 0) \right. \\ &\quad \times \left. \left. C_e \tilde{P}(x', \mathcal{T}^{-1}|x_0, 0) \right\} \left\{ \left[1 + C\tilde{P}(x', \mathcal{T}^{-1}|x', 0) \right] \right. \right. \\ &\quad \times \left. \left. \left[1 + C_e \tilde{P}(x_e, \mathcal{T}^{-1}|x_e, 0) \right] - C\tilde{P}(x_e, \mathcal{T}^{-1}|x', 0) C_e \tilde{P}(x', \mathcal{T}^{-1}|x_e, 0) \right\}^{-1} \right), \end{aligned} \quad (30)$$

and with $\tilde{P}_{\text{reset}}(y, s|z, 0)$ replacing $\tilde{P}(y, s|z, 0)$ for the reset model.

In Fig. 4, where we plot $\tilde{\phi}(0)$ as a function of the strength of the interaction $\Gamma = v|x_e - x_c|/D$ for the drift model and $\Gamma = \sqrt{r/D}|x_e - x_c|$ for the reset model, the non-monotonicity appears clearly and is more visible the larger is the dimensionless rate $R = |x_e - x_c|\sqrt{\mathcal{T}^{-1}/D}$. For the reset model the minimum of $\phi(0)$ shifts towards larger value as Γ increases while it does not move appreciably for the drift model. This can be understood by noticing that R is proportional with $\sqrt{\mathcal{T}}$. As Γ is also proportional to a rate, i.e. \sqrt{r} , two decay processes may compete. As the minimum of the yield corresponds to when a particle has had the largest number of chances of being absorbed by the trap, an increase in \mathcal{T} would limit those chances causing $\tilde{\phi}(0)$ to increase across

all values of Γ . But that decay competes with the decay r , while it does not in the drift model since the bias is deterministic and thus has no effect on the location of the minimum yield.

For most values of Γ the yield of the reset model is lower than the one for the drift model due to the weaker confinement of the resetting walker compared to the biased walker. This larger exploratory propensity, that is the tendency to stray further away from the focal point of the reset model in comparison to the drift model, as also indicated by the MSD (Fig. 3), is also responsible, as we will see in Sec. 4, for the quantitative differences in the values of mean first-passage times.

4. First-passage processes

In presence of a single trap at $x = x'$ we can determine the survival probability $M(t)$ by integrating the probability distribution at the trap site, given in Eq. (24), over all space and obtain

$$\widetilde{M}(\epsilon) = \frac{1}{\epsilon + \tau^{-1}} \left[1 - \frac{\widetilde{P}(x', \epsilon + \tau^{-1}|x_0, 0)}{1/C + \widetilde{P}(x', \epsilon + \tau^{-1}|x', 0)} \right], \quad (31)$$

where it is assumed that $x_0 \neq x'$. In the limit $\tau^{-1} \rightarrow 0$ and $C \rightarrow +\infty$, that is for the case of a perfectly absorbing trap at x' Eq. (31) reduces to the Laplace expression of the relation between the first-passage probability distribution from x_0 to x' and the survival probability, namely $-\epsilon \widetilde{M}(\epsilon) + M(0) = \widetilde{\mathcal{F}}(x', \epsilon|x_0)$ with $M(0) = 1$, or its time equivalent relation $-dM(t)/dt = \mathcal{F}(x', t|x_0)$.

The first-passage distribution $\mathcal{F}(x, t|x_0)$ from x_0 to x for the two models can be expressed as

$$\widetilde{\mathcal{F}}(x, \epsilon|x_0) = \frac{h_{x_c}(x, x_0) \mathcal{C}(\epsilon) e^{-\alpha|x-x_0|S(\epsilon)} + \mathcal{D}_{x_c}(x_0, \epsilon) e^{-\alpha|x-x_c|S(\epsilon)}}{h_{x_c}(x, x) \mathcal{C}(\epsilon) + \mathcal{D}_{x_c}(x, \epsilon) e^{-\alpha|x-x_c|S(\epsilon)}} \quad (32)$$

from which the mean first-passage time (MFPT) $\langle t_F(x|x_0) \rangle$ to reach x from x_0 is obtained by performing $-\partial \mathcal{F}(x, \epsilon|x_0)/\partial \epsilon \Big|_{\epsilon=0}$. After some algebra one can show that the general expression is

$$\langle t_F(x|x_0) \rangle = \frac{h_{x_c}(x, x_0) e^{\alpha|x-x_c|S(0)}}{h_{x_c}(x, x) \mathcal{D}_{x_c}^2(x, 0)} \left\{ \mathcal{C}'(0) [\mathcal{D}_{x_c}(x_0, 0) - \mathcal{D}_{x_c}(x, 0) e^{-\alpha|x-x_0|S(0)}] \right. \\ \left. + e^{-\alpha|x-x_c|S(0)} [\mathcal{D}'_{x_c}(x, 0) \mathcal{D}_{x_c}(x_0, 0) - \mathcal{D}'_{x_c}(x_0, 0) \mathcal{D}_{x_c}(x, 0)] \right\}. \quad (33)$$

Using Eq. (20) the general expression above can be written explicitly for the constant drift model as

$$\langle t_F(x|x_0) \rangle = \frac{2D}{v^2} \left\{ e^{\frac{v|x-x_c|}{D}} \left[1 - e^{\frac{v(|x_0-x_c|-|x-x_0|-|x-x_c|)}{2D}} \right] + \frac{v(|x_0-x_c|-|x-x_c|)}{2D} \right\}. \quad (34)$$

The form of Eq. (34) indicates that the time to reach a target is composed of two contributions. For clarity of explanation, let us suppose that $x_c < x < x_0$. In such a scenario, one finds that $\langle t_F(x|x_0) \rangle = \frac{|x_0-x_c|-|x-x_c|}{v}$, that is, the mean first-passage time is simply the time it takes the mean position of the walker, initially at x_0 , to reach x_c

moving at speed v . To consider the other case with $x > x_0$, let us first look at the case $x_0 = x_c$, for which

$$\langle t_F(x|x_c) \rangle = \frac{2D}{v^2} \left[e^{\frac{v|x-x_c|}{D}} - 1 - \frac{1}{2} \frac{v|x-x_c|}{D} \right]. \quad (35)$$

With (35), we can now see that the case in which $x > x_0$ with $x, x_0 > x_c$, the mean first-passage time is

$$\langle t_F(x|x_0) \rangle = \langle t_F(x|x_c) \rangle - \langle t_F(x_0|x_c) \rangle, \quad (36)$$

that is, the average time one would need to get to x from x_c minus the contribution to get to x_0 from x_c . If $x_0 < x_c$ but $x > x_c$, then $\langle t_F(x|x_0) \rangle = \langle t_F(x|x_c) \rangle + \langle t_F(x_c|x_0) \rangle$, that is, the contribution is the average time to get to x_c added to the average time to reach x from x_c .

A natural comparison of the MFPT from x_c to a target at x in presence of a potential may be made with the diffusive time between x and x_c , that is $(x-x_c)^2/(2D)$. Denoting the ratio of the two by $g\left(\frac{v|x-x_c|}{D}\right)$, we have for the constant drift model

$$g(z) = \frac{4}{z^2} \left(e^z - 1 - \frac{z}{2} \right). \quad (37)$$

For a fixed $|x-x_c|$ and D , as Eq. (37) diverges both for $z \rightarrow 0$ and $z \rightarrow +\infty$, $g(z)$ possess a minimum. The divergence for small z is expected as for $v \rightarrow 0$ the problem reduces to the unconstrained Brownian walker whose MFPT between any two points is infinite. The opposite limit, for very large z , that is when $v \rightarrow +\infty$, diverges because a point away from x_c will never be reached. There is therefore an intermediate value of v for which $g(z)$ is minimal. That value can be computed numerically from Eq. (37) and equals $z^* \simeq 1.245$.

For the resetting case, using the expressions in (21) in Eq. (34), it follows that the MFPT

$$\langle t_F(x|x_0) \rangle = \frac{e^{|x-x_c|\sqrt{r/D}}}{r} \left(1 - e^{-|x-x_0|\sqrt{r/D}} \right). \quad (38)$$

The dimensionless expression $g\left(|x-x_c|\sqrt{r/D}\right) = 2D\langle t_F(x|x_c) \rangle / (x-x_c)^2$ that represents a walker reaching x for the first time while starting from $x_0 = x_c$ can be written as

$$g(z) = 2 \frac{e^z - 1}{z^2}. \quad (39)$$

Similarly to the drift model for a given fixed $|x-x_c|$ and a given diffusion constant, the above expression implies a finite MFPT at a finite r , and a divergence at the two limits $r \rightarrow 0$ (pure diffusion) and $r \rightarrow +\infty$. In the latter case, too frequent resets for the motion to reach the target in between lead to an infinite MFPT. In fact, as a function of r , the MFPT has its minimum at an optimal resetting rate $r_{\text{opt}} = (z^*)^2 D / |x-x_0|^2$, where z^* solves the transcendental equation $z^*/2 = 1 - e^{-z^*}$, and has the numerical value $z^* = 1.59362\dots$ [25].

The comparison of Eqs. (37) and (39) for the dimensionless $g(z)$ displays the minima for both models. The plot in Fig. 5 also indicates that the MFPT from x_c to any point in space for the drift model is always larger than the corresponding one for the reset model. As mentioned already in presenting the quantum yield in Sec. 3, this is the result of the comparatively weaker tendency of the reset model to return to x_c . Note that the results summarized in Fig. 5 have already been reported earlier in Ref. [6] by the approach of backward Fokker-Planck equation.

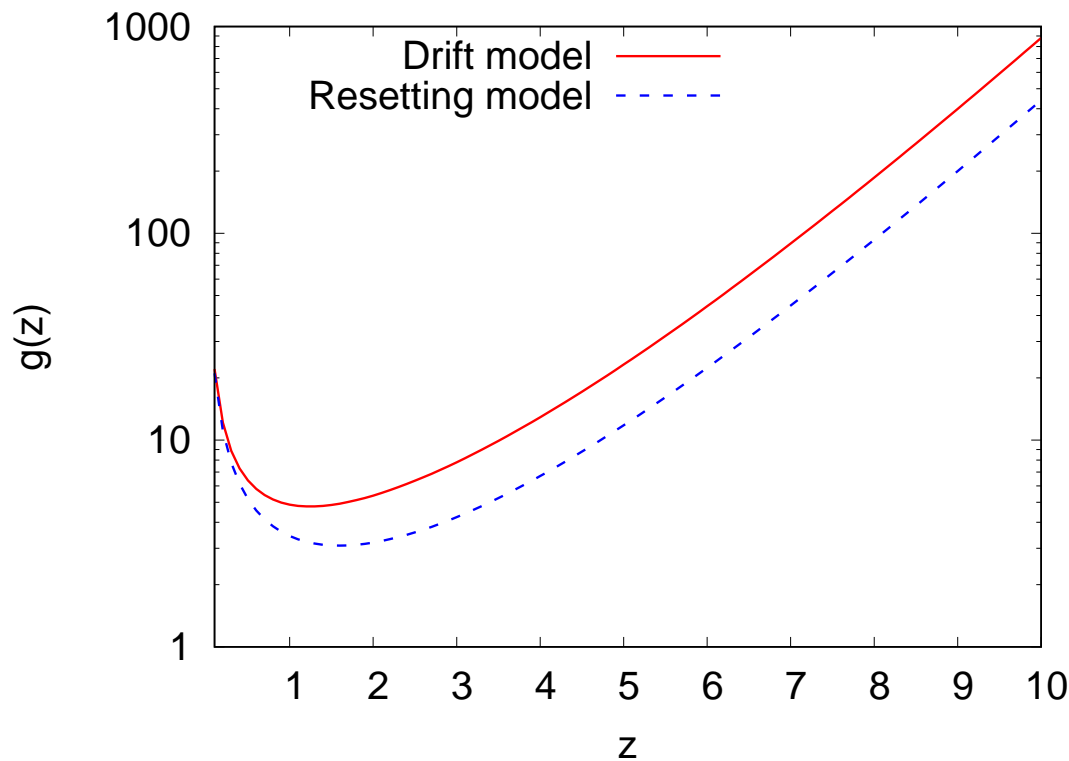


Figure 5. (Color online) Comparison of the dimensionless MFPT for the constant drift model and the resetting model. Here, $z = \frac{v|x-x_c|}{D}$ for the drift model, while $z = \frac{|x-x_c|\sqrt{r}}{\sqrt{D}}$ for the resetting model. The function $g(z)$ is given by Eq. (37) for the drift model and by Eq. (39) for the resetting model.

5. Splitting probability and propagators in presence of two absorbing targets

A natural extension of the case $C \rightarrow +\infty$ for one trap is the problem of two absorbing defects. It corresponds to Eqs. (27) and (28) with C , C_e , τ and τ_e infinitely large. As the method of images can only be applied when the space is homogeneous, the presence of a focal point forces us to employ a different methodology. We analyze in particular the situation when one defect is at $x = a$ and the other at $x = b$, respectively, to the left and to the right of the focal point (for simplicity $x_c = 0$), and with the initial location of

the walker being $a < x_0 < b$. Following Ref. [26], we proceed by constructing the general expression for the propagator in presence of these absorbing boundaries. We start first with the case of a single absorbing boundary at $x = a$. One takes the propagator without boundaries $P(x, t|x_0)$ and constructs the one in presence of the absorbing boundary by subtracting all the trajectories that go through $x = a$ at some time $t' < t$. Denoting by $Q_a(x, t|x_0)$ the distribution for the ensemble of such trajectories, we can determine it by relating it to $P(x, t|x_0, 0)$ and $P(x, t|a, 0)$ via the first-passage probability $\mathcal{F}(a, t|x_0)$ to be at x at some time t starting at x_0 . In fact, we have that $\mathcal{F}(a, s|x_0)P(x, t-s|a)$ represents the probability distribution of having reached $x = a$ at time s (earlier than t) and subsequently having reached x at time t starting from $x = a$. Integrating up to time t gives the relation $H_a(x, t|x_0) = \int_0^t ds \mathcal{F}(a, s|x_0)P(x, t-s|a)$. If we now subtract $H_a(x, t|x_0)$ from $P(x, t|x_0)$, we have the probability of all trajectories that are at x at time t that have not reached a at an earlier time. In Laplace space, we simply write

$$\tilde{\mathcal{A}}_a(x, \epsilon|x_0) = \tilde{P}(x, \epsilon|x_0) - \tilde{\mathcal{F}}(a, \epsilon|x_0)\tilde{P}(x, \epsilon|a), \quad (40)$$

which is the Laplace propagator for the walker being at x at time t starting at x_0 in presence of an absorbing boundary at $x = a$.

We now consider the other absorbing boundary at $x = b$ and we determine the probability of having reached b without having gone through $x = a$ and vice versa. Let us call $\mathcal{G}_a(b, t|x_0)$ the probability density of having reached b at time t without having been at $x = a$ at an earlier time. We can now use the propagator $\mathcal{A}_a(x, t|x_0)$ to do it since we use the relation

$$\mathcal{A}_a(b, t|x_0) = \int_0^t ds \mathcal{G}_a(b, s|x_0)\mathcal{A}_a(b, t-s|b). \quad (41)$$

Eq. (41) is analogous to what used earlier to define a relation between first-passage at $x = b$ and probability distribution to be at x at time t . That general relation is here employed with the propagator in presence of an absorbing boundary at a in place of the usual propagator P in the absence of any boundary. In Laplace it is simply $\tilde{\mathcal{A}}_a(b, \epsilon|x_0) = \tilde{\mathcal{G}}_a(b, \epsilon|x_0)\tilde{\mathcal{A}}_a(b, \epsilon|b)$. We can thus write

$$\tilde{\mathcal{G}}_a(b, \epsilon|x_0) = \frac{\tilde{\mathcal{A}}_a(b, \epsilon|x_0)}{\tilde{\mathcal{A}}_a(b, \epsilon|b)}. \quad (42)$$

We can similarly construct the case in which we consider first the absorbing boundary at $x = b$ for which we write the propagator as

$$\tilde{\mathcal{A}}_b(x, \epsilon|x_0) = \tilde{P}(x, \epsilon|x_0) - \tilde{\mathcal{F}}(b, \epsilon|x_0)\tilde{P}(x, \epsilon|b), \quad (43)$$

and similarly

$$\tilde{\mathcal{G}}_b(a, \epsilon|x_0) = \frac{\tilde{\mathcal{A}}_b(a, \epsilon|x_0)}{\tilde{\mathcal{A}}_b(a, \epsilon|a)}. \quad (44)$$

In extended form we have that

$$\tilde{\mathcal{G}}_a(b, \epsilon|x_0) = \frac{\tilde{P}(b, \epsilon|x_0) - \tilde{\mathcal{F}}(a, \epsilon|x_0)\tilde{P}(b, \epsilon|a)}{\tilde{P}(b, \epsilon|b) - \tilde{\mathcal{F}}(a, \epsilon|b)\tilde{P}(b, \epsilon|a)}, \quad (45)$$

and

$$\tilde{\mathcal{G}}_b(a, \epsilon|x_0) = \frac{\tilde{P}(a, \epsilon|x_0) - \tilde{\mathcal{F}}(b, \epsilon|x_0)\tilde{P}(a, \epsilon|b)}{\tilde{P}(a, \epsilon|a) - \tilde{\mathcal{F}}(b, \epsilon|a)\tilde{P}(a, \epsilon|b)}, \quad (46)$$

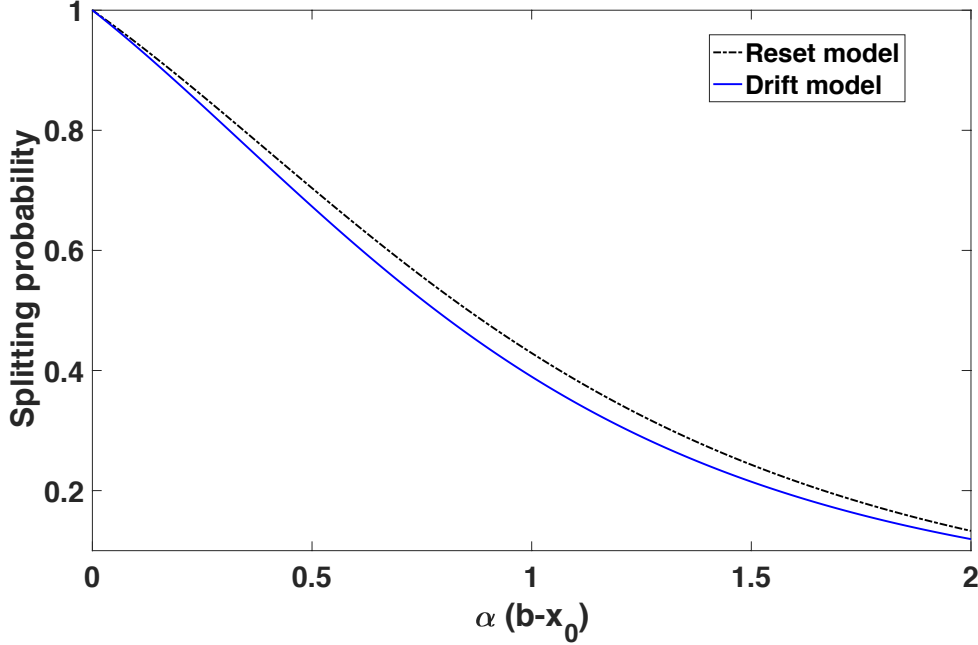


Figure 6. (Color online) Comparison of the splitting probability $\tilde{\mathcal{G}}_a(b, 0|x_0)$ for the two models, namely the probability of reaching $x = b$ without ever reaching $x = a$. The focal point is set at $\alpha x_c = 0$, the initial condition at $\alpha x_0 = 2$ and $\alpha|b - a| = 4$. The data is generated by a rigid translation of a and b to the right in Eqs. (47) and (48) for the drift and reset model, respectively. The higher splitting probability for the reset model is another indication of the stronger exploratory nature of its walk compared to the drift model.

with the latter expression also derivable from the former by a simple exchange of a and b . While we have reported the explicit form of Eq. (45) in Appendix C in Eq. (C1), we write here explicitly the quantities $\tilde{\mathcal{G}}_a(b, 0|x_0)$ and $\tilde{\mathcal{G}}_b(a, 0|x_0)$ (notice that $\tilde{\mathcal{G}}_a(b, 0|x_0) + \tilde{\mathcal{G}}_b(a, 0|x_0) = 1$), which are the so-called splitting probabilities, respectively, of reaching b without having reached a , and of reaching a without having reached b . For the drift model we have

$$\tilde{\mathcal{G}}_a(b, 0|x_0) = \frac{e^{-\frac{v|b|}{D}} - e^{-\frac{v(|b|+|a|+|b-a|)}{2D}} + e^{-\frac{v(|b|+2|a|+|b-x_0|-|x_0|)}{2D}} - e^{-\frac{v(|a|+2|b|+|a-x_0|-|x_0|)}{2D}}}{e^{-\frac{v|a|}{D}} + e^{-\frac{v|b|}{D}} - 2e^{-\frac{v(|a|+|b|+|b-a|)}{2D}}}, \quad (47)$$

while for the reset model we obtain the expression

$$\tilde{\mathcal{G}}_a(b, 0|x_0) = \frac{e^{|b-a|\sqrt{r/D}} \left(e^{(|b|-|b-x_0|)\sqrt{r/D}} - e^{(|a|-|a-x_0|)\sqrt{r/D}} \right) + e^{(|a|+|b-a|)\sqrt{r/D}} - e^{|b|\sqrt{r/D}}}{\left(e^{|b-a|\sqrt{r/D}} - 1 \right) \left(e^{|a|\sqrt{r/D}} + e^{|b|\sqrt{r/D}} \right)}. \quad (48)$$

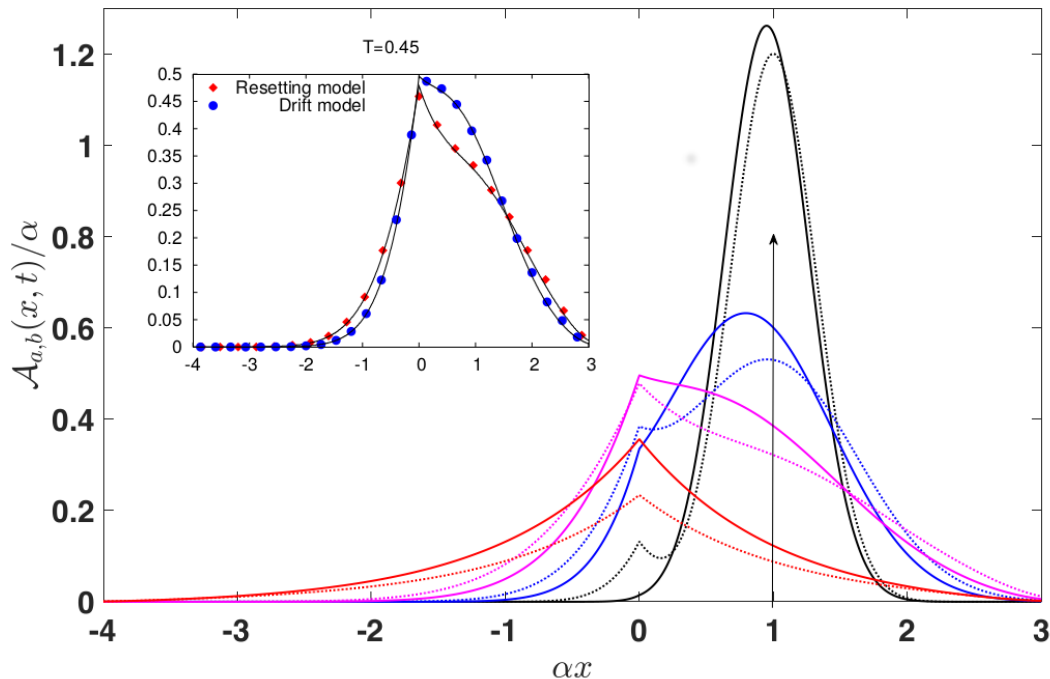


Figure 7. (Color online) Comparison of the spatio-temporal dynamics of $\mathcal{A}_{a,b}(x, t)$ with $x_c = 0$ for the constant drift model (solid lines) and the reset model (dashed lines) in presence of two absorbing boundaries at $x = a$ and $x = b$. The Dirac delta initial condition, indicated by the arrow, is located at $\alpha x_0 = 1$ and the left and right boundaries are, respectively, at $\alpha a = -4$ and $\alpha b = 3$. Starting from the highest curves on the right, the different lines for the two models are plotted at times $T = 0.05, 0.2, 0.45,$ and 9.95 . The inset shows the match between theory and simulations for $T = 0.45$.

Analogously to the differences observed for the MSD, the quantum yield and the MFPT analysis, we expect the splitting probability to be higher for the reset model compared to the drift model because a walker subject to a deterministic drift is more likely to roam closer to x_c and thus reduce the chance of encountering the forbidden target. This difference is shown in Fig. 6 where we plot the splitting probability $\tilde{\mathcal{G}}_a(b, 0|x_0)$.

To determine the general propagator $\tilde{\mathcal{A}}_{a,b}(x, \epsilon|x_0)$ in presence of an absorbing boundary at $x = a$ and $x = b$ it is necessary to subtract from the free propagation the contribution of those trajectories that reach first $x = a$ before reaching $x = b$ and those that reach $x = b$ before reaching $x = a$. The resulting propagator is

$$\tilde{\mathcal{A}}_{a,b}(x, \epsilon|x_0) = \tilde{P}(x, \epsilon|x_0) - \tilde{\mathcal{G}}_a(b, \epsilon|x_0)\tilde{P}(x, \epsilon|b) - \tilde{\mathcal{G}}_b(a, \epsilon|x_0)\tilde{P}(x, \epsilon|a), \quad (49)$$

which by construction is identically zero at $x = a$ and $x = b$. The dynamics of $\mathcal{A}_{a,b}(x, t|x_0)$ for the two models is displayed in Fig. 7.

6. Conclusions

We have presented a systematic analysis of two models of tethered motion. The analytic knowledge of the propagators for the two processes has been instrumental in our findings. We have shown how the fundamental difference of the two models, that is, the biased movement through the intervening space for the drift model versus the random and sudden jumps to the focal point for the resetting model, affects the dynamics of the walker. We have demonstrated the effects by not only comparing the spatio-temporal dynamics of the propagators, but also deriving quantities such as the mean first-passage time, splitting probabilities, and the probability distribution in presence of absorbing boundaries.

Compared to the resetting model, the deterministic nature of the bias in the drift model limits the spatial extent over which the walker moves away from the focal point. In other words the two models exhibit a different exploratory dynamics around the focal point. As the possibility for larger exploration favors the walker to cover the available space, search for a randomly located item is more efficient with the reset model, as shown by the analysis of the mean first-passage time. For the same reason, a better performance of the reset model for random search of multiple targets is also expected, as shown by our comparison of the splitting probabilities of perfectly absorbing targets. Calculations for the quantum yield with a guest molecule and a trap, both away from the focal point, shows that the drift model for different choices of absorption reaches higher values for most cases of confinement strength because the absorbing targets are reached less often when compared to the reset model.

The formalism developed here for the drift model has applications in studying animal movement where the model is well known since the '70s, [9], under the name Holgate-Okubo model [27]. It was introduced in the literature to model many examples of animal roaming within their own home range and for which a focal point represents a burrow or a den site, while the tendency to return is represented by biasing the random movement with a drift. Despite its long history, it is only recently that the derivation of an analytic expression for the propagator has been achieved, first in 2010 [7] and, through a different technique, in 2016 [8] by some of the present authors.

Despite its simplicity, the Holgate-Okubo model has been extensively employed to model confined animal movement, and many variants have appeared over the years. A simple way to introduce variation to the model is to change the confining potential—proportional to the modulus of the distance from the focal point in the drift model—to a shallower or steeper spatial profile [28]. One example is the use of a quadratic potential, whereby the Fokker-Planck equation of the drift model reduces to that of the Ornstein-Uhlenbeck process [29] representing the noisy, overdamped dynamics of a walker being pulled towards the focal point by a harmonic spring.

The history of the stochastic resetting model is instead much more recent. It has emerged in recent years as an interesting and an analytically tractable paradigm to study stationary processes out of equilibrium. A variety of situations have been

considered, e.g., a diffusing particle resetting to its initial position in either a free [4, 5, 30, 31, 32, 33], or a bounded domain [34], in presence of an external potential [35], and for different choices of the resetting position [25, 36, 37]. Other generalizations include resetting of continuous-time random walks [38, 39], Lévy [40] and exponential constant-speed flights [41], and time-dependent resetting of a Brownian particle [42]. Stochastic resetting has also been invoked in the context of reaction-diffusion models [43], fluctuating interfaces [44, 45], in modeling backtrack recovery by RNA polymerases [46], and in discussing stochastic thermodynamics far from equilibrium [47]. Various static and time-dependent aspects of resetting dynamics have been studied over the years, e.g., in discussing first-passage properties [48], optimal search strategies [49, 50, 51] and first-arrival times [52], and resetting in a bounded domain [53, 54]. A recent study of resetting, invoking the path-integral formalism of stochastic processes, has shown how resetting may have practical applications in confining diffusing particles in space. For example, it was demonstrated in the case of energy-dependent resetting in presence of a harmonic potential that a specified degree of spatial confinement of Brownian particles is possible on a much faster time scale than what may be achieved by performing quenches of parameters of the harmonic potential [55]. Other possible applications of our reset formalism could be in discussing the contracted movement of a random walker from a higher dimensional space with effective long range jumps. A typical example would be the diffusion onto a DNA sequence [56]. On one hand, two bases might be very far from each other, if some substance has to be transported along the sequence. On the other hand, the two base may be considered just a single step away if the coiling of the DNA in three dimensions makes the two base touch each other. We wrap off by mentioning future directions to pursue that could include extending our analysis to consider the presence of reflecting boundary conditions, dynamics in higher dimensions, as well as the case of many interacting random walkers.

Appendix A

For completeness we report the MSD expression for the drift model for the general case with x_0 and x_c not identically zero. The calculation proceeds in two steps given that the propagator in Eq. (7) can be expressed as the sum of two terms $P_1(x, t)$ and $P_2(x, t)$, the latter being the term containing the error function. For the first term one needs to integrate

$$\begin{aligned} I_1(t) &= \int_{-\infty}^{+\infty} dx (x - x_0)^2 P_1(x, t) \\ &= F(x_0, x_c, t) \int_0^{+\infty} dy e^{-\frac{y^2}{4Dt} - \frac{vy}{2D}} \left\{ [2\gamma^2 + 2y^2] \cosh\left(\frac{y\gamma}{2Dt}\right) - 4\gamma y \sinh\left(\frac{y\gamma}{2Dt}\right) \right\}, \end{aligned} \quad (\text{A1})$$

with $F(x_0, x_c, t) = \frac{1}{4\pi Dt} e^{\frac{v|x_c-x_0|}{2D} - \frac{v^2 t}{4D} - \frac{(x_c-x_0)^2}{4Dt}}$ and $\gamma = x_c - x_0$, whereas for the second term the integration reduces to the calculation of the integral

$$I_2(t) = \int_{-\infty}^{+\infty} dx (x - x_0)^2 P_2(x, t)$$

$$= \frac{v}{2} \sqrt{\frac{t}{D}} \int_0^{+\infty} dy e^{-2yv\sqrt{\frac{t}{D}}} (4Dty^2 + \gamma^2) \operatorname{Erfc} \left(y + \frac{|\gamma| - vt}{\sqrt{4Dt}} \right). \quad (\text{A2})$$

Performing the integrations give

$$I_1(t) = -\frac{2}{\sqrt{\pi}} \sqrt{Dt} vt e^{-\frac{1}{4}(\sqrt{\frac{t}{D}}v - \frac{|\gamma|}{\sqrt{Dt}})^2} + \left(Dt + \frac{v^2 t^2}{2} \right) \times \left\{ e^{\frac{v(|\gamma| - \gamma)}{2D}} \operatorname{Erfc} \left[\frac{1}{2} \left(\sqrt{\frac{t}{D}}v - \frac{\gamma}{\sqrt{Dt}} \right) \right] + e^{\frac{v(|\gamma| + \gamma)}{2D}} \operatorname{Erfc} \left[\frac{1}{2} \left(\sqrt{\frac{t}{D}}v + \frac{\gamma}{\sqrt{Dt}} \right) \right] \right\}, \quad (\text{A3})$$

and

$$I_2(t) = 2 \frac{D^2}{v^2} + \gamma^2 + \left[\sqrt{\frac{Dt}{\pi}} \left(|\gamma| + vt - 2 \frac{D}{v} \right) e^{-\frac{1}{4}(\sqrt{\frac{t}{D}}v - \frac{|\gamma|}{\sqrt{Dt}})^2} - \operatorname{Erfc} \left[\frac{1}{2} \left(\sqrt{\frac{t}{D}}v - \frac{|\gamma|}{\sqrt{Dt}} \right) \right] \right] \times \left(\frac{D^2}{v^2} + \frac{\gamma^2}{2} \right) - e^{\frac{v|\gamma|}{D}} \left\{ vt|\gamma| + \frac{D^2}{v^2} \left(1 - \frac{v|\gamma|}{D} \right) + \frac{v^2 t^2}{2} + \frac{\gamma^2}{2} \right\} \operatorname{Erfc} \left[\frac{1}{2} \left(\sqrt{\frac{t}{D}}v + \frac{|\gamma|}{\sqrt{Dt}} \right) \right]. \quad (\text{A4})$$

Combining Eq. (A3) and (A4) one obtains

$$\langle (x - x_0)^2 \rangle(t) = 2 \frac{D^2}{v^2} + \gamma^2 + \left[\sqrt{\frac{Dt}{\pi}} \left(|\gamma| - vt - 2 \frac{D}{v} \right) e^{-\frac{1}{4}(\sqrt{\frac{t}{D}}v - \frac{|\gamma|}{\sqrt{Dt}})^2} + \left(Dt + \frac{v^2 t^2}{2} - \frac{D^2}{v^2} - \frac{\gamma^2}{2} \right) \operatorname{Erfc} \left[\frac{1}{2} \left(\sqrt{\frac{t}{D}}v - \frac{|\gamma|}{\sqrt{Dt}} \right) \right] + e^{\frac{v|\gamma|}{D}} \left\{ Dt - vt|\gamma| - \frac{D^2}{v^2} \left(1 - \frac{v|\gamma|}{D} \right) - \frac{\gamma^2}{2} \right\} \operatorname{Erfc} \left[\frac{1}{2} \left(\sqrt{\frac{t}{D}}v + \frac{|\gamma|}{\sqrt{Dt}} \right) \right] \right], \quad (\text{A5})$$

which reduces to the one reported in the main text in Eq. (10).

Appendix B

To determine the exact form of $\tilde{\mathcal{P}}_e(x_e, \epsilon | x_0, 0)$ and $\tilde{\mathcal{P}}_e(x', \epsilon | x_0, 0)$ in Sec. 3 we assign $x = x'$ and $x = x_e$ to $\tilde{\mathcal{P}}_e(x, \epsilon + \mathcal{T}^{-1} | x_0, 0)$ in Eq. (29) and we are left to solve the matricial equation

$$\begin{pmatrix} 1 + C\tilde{P}(x', \epsilon + \mathcal{T}^{-1} | x', 0) & C_e\tilde{P}(x', \epsilon + \mathcal{T}^{-1} | x_e, 0) \\ C\tilde{P}(x_e, \epsilon + \mathcal{T}^{-1} | x', 0) & 1 + C_e\tilde{P}(x_e, \epsilon + \mathcal{T}^{-1} | x_e, 0) \end{pmatrix} \begin{pmatrix} \tilde{\mathcal{P}}_e(x', \epsilon | x_0, 0) \\ \tilde{\mathcal{P}}_e(x_e, \epsilon | x_0, 0) \end{pmatrix} = \begin{pmatrix} \tilde{P}(x', \epsilon + \mathcal{T}^{-1} | x_0, 0) \\ \tilde{P}(x_e, \epsilon + \mathcal{T}^{-1} | x_0, 0) \end{pmatrix}. \quad (\text{B1})$$

Inverting the matrix allows us to determine $\tilde{\mathcal{P}}_e(x_e, \epsilon | x_0, 0)$ and $\tilde{\mathcal{P}}_e(x', \epsilon | x_0, 0)$ and thus obtain the general expression for $\tilde{\mathcal{P}}_e(x, \epsilon | x_0, 0)$ in Eq. (29), namely

$$\tilde{\mathcal{P}}_e(x, \epsilon | x_0, 0) = \tilde{P}(x, \epsilon + \mathcal{T}^{-1} | x_0, 0) - C\tilde{P}(x, \epsilon + \mathcal{T}^{-1} | x', 0) \left\{ \left[1 + C_e\tilde{P}(x_e, \epsilon + \mathcal{T}^{-1} | x_e, 0) \right] \times \tilde{P}(x', \epsilon + \mathcal{T}^{-1} | x_0, 0) - C_e\tilde{P}(x', \epsilon + \mathcal{T}^{-1} | x_e, 0) \tilde{P}(x_e, \epsilon + \mathcal{T}^{-1} | x_0, 0) \right\} \mathcal{A}(\epsilon)$$

$$\begin{aligned}
& - C_e \tilde{P}(x, \epsilon + \mathcal{T}^{-1}|x_e, 0) \left\{ \left[1 + C\tilde{P}(x', \epsilon + \mathcal{T}^{-1}|x', 0) \right] C\tilde{P}(x_e, \epsilon + \mathcal{T}^{-1}|x_0, 0) \right. \\
& \left. - C\tilde{P}(x_e, \epsilon + \mathcal{T}^{-1}|x', 0) \tilde{P}(x', \epsilon + \mathcal{T}^{-1}|x_0, 0) \right\} \mathcal{A}(\epsilon), \tag{B2}
\end{aligned}$$

where

$$\begin{aligned}
\mathcal{A}(\epsilon) = & \left\{ \left[1 + C\tilde{P}(x', \epsilon + \mathcal{T}^{-1}|x', 0) \right] \left[1 + C_e \tilde{P}(x_e, \epsilon + \mathcal{T}^{-1}|x_e, 0) \right] \right. \\
& \left. - C\tilde{P}(x_e, \epsilon + \mathcal{T}^{-1}|x', 0) C_e \tilde{P}(x', \epsilon + \mathcal{T}^{-1}|x_e, 0) \right\}^{-1}. \tag{B3}
\end{aligned}$$

In the absence of traps or guest molecule and the associated probability decay, that is respectively with $C_e \rightarrow 0$ and $\tau_e \rightarrow +\infty$ or $C \rightarrow 0$ and $\tau \rightarrow +\infty$, the form of the propagator reduces to the one found in Eq. (24).

Appendix C

Here we explicitly show the Laplace expression (42) for the splitting probability distribution $\mathcal{G}_a(b, \epsilon|x_0)$, that is the probability distribution of reaching $x = b$ without having reached $x = a$. With the notation explained in Sec. 2 it is given by

$$\begin{aligned}
\mathcal{G}_a(b, \epsilon|x_0) = & h_{x_c}(b, x_0) \left\{ \mathcal{C}(\epsilon) \left[e^{-\alpha|b-x_0|\mathcal{S}(\epsilon)} - e^{-\alpha(|a-x_0|+|a-b|\mathcal{S}(\epsilon))} \right] + \mathcal{D}_{x_c}(a, \epsilon) \left[e^{-\alpha(|b-x_0|+|a|\mathcal{S}(\epsilon))} \right. \right. \\
& \left. \left. - e^{-\alpha(|a-x_0|+|b|\mathcal{S}(\epsilon))} \right] + \mathcal{D}_{x_c}(x_0, \epsilon) \left[e^{-\alpha|b|\mathcal{S}(\epsilon)} - e^{-\alpha(|a-b|+|a|\mathcal{S}(\epsilon))} \right] \right\} \left\{ \mathcal{C}(\epsilon) \left[1 - e^{-2\alpha|a-b|\mathcal{S}(\epsilon)} \right] \right. \\
& \left. + \mathcal{D}_{x_c}(a, \epsilon) \left[e^{-\alpha|a|\mathcal{S}(\epsilon)} - e^{-\alpha(|a-b|+|b|\mathcal{S}(\epsilon))} \right] + \mathcal{D}_{x_c}(b, \epsilon) \left[e^{-\alpha|b|\mathcal{S}(\epsilon)} - e^{-\alpha(|a-b|+|a|\mathcal{S}(\epsilon))} \right] \right\}. \tag{C1}
\end{aligned}$$

It is this expression for $\mathcal{G}_a(b, \epsilon|x_0)$ and the corresponding $\mathcal{G}_b(a, \epsilon|x_0)$ that we have Laplace inverted and then convoluted, respectively, with the known time-dependent functions $\tilde{P}(x, \epsilon|b)$ and $\tilde{P}(x, \epsilon|a)$ to reconstruct the probability distribution and plot $\mathcal{A}_{a,b}(x, t|x_0)$ in Fig. 7.

Appendix D

The expression for the survival probability studied in Sec. 5 requires knowledge of certain finite integrals. They are

$$\int_a^b dx e^{-\beta|x-\alpha|} = \text{sign}(b-\alpha) \frac{1 - e^{-\beta|b-\alpha|}}{\beta} - \text{sign}(a-\alpha) \frac{1 - e^{-\beta|a-\alpha|}}{\beta}, \tag{D1}$$

and

$$\begin{aligned}
& \int_a^b dx e^{-\delta|x-x_0|-\beta|x|} = e^{-\delta x_0} \int_a^{x_0} dx e^{\delta x - \beta|x|} + e^{\delta x_0} \int_{x_0}^b dx e^{-\delta x - \beta|x|} \\
= & e^{-\delta x_0} \left[\frac{1 - e^{\delta a - \beta|a|}}{\delta - \beta \text{sign}(a)} - \frac{1 - e^{\delta x_0 - \beta|x_0|}}{\delta - \beta \text{sign}(x_0)} \right] + e^{\delta x_0} \left[\frac{e^{-\delta x_0 - \beta|x_0|} - 1}{\delta + \beta \text{sign}(x_0)} + \frac{1 - e^{-\delta b - \beta|b|}}{\delta + \beta \text{sign}(b)} \right] \\
= & e^{-\delta x_0} \left[\frac{1 - e^{a[\delta - \beta \text{sign}(a)]}}{\delta - \beta \text{sign}(a)} - \frac{1 - e^{x_0[\delta - \beta \text{sign}(x_0)]}}{\delta - \beta \text{sign}(x_0)} \right] \\
& + e^{\delta x_0} \left[\frac{e^{-x_0[\delta + \beta \text{sign}(x_0)]} - 1}{\delta + \beta \text{sign}(x_0)} + \frac{1 - e^{-b[\delta + \beta \text{sign}(b)]}}{\delta + \beta \text{sign}(b)} \right]. \tag{D2}
\end{aligned}$$

For the exponential reset we have

$$\int_a^b dx \tilde{P}(x, \epsilon|a) = \frac{1}{\sqrt{2}(r + \epsilon)} \left\{ \frac{r}{\epsilon} \left[2 - e^{-b\sqrt{(r+\epsilon)/D}} - e^{a\sqrt{(r+\epsilon)/D}} \right] + 1 - e^{-(b-a)\sqrt{(r+\epsilon)/D}} \right\} \quad (\text{D3})$$

and

$$\tilde{\mathcal{G}}_a(b, \epsilon|x_0) = \frac{r e^{-b\sqrt{(r+\epsilon)/D}} + \epsilon e^{-(b-x_0)\sqrt{(r+\epsilon)/D}} - \tilde{\mathcal{F}}(a, \epsilon|x_0) \left[r e^{-b\sqrt{(r+\epsilon)/D}} + \epsilon e^{-(b-a)\sqrt{(r+\epsilon)/D}} \right]}{r e^{-b\sqrt{(r+\epsilon)/D}} + \epsilon - \tilde{\mathcal{F}}(a, \epsilon|b) \left[r e^{-b\sqrt{(r+\epsilon)/D}} + \epsilon e^{-(b-a)\sqrt{(r+\epsilon)/D}} \right]}. \quad (\text{D4})$$

By taking the limit $\epsilon \rightarrow 0$ in Eq. (D4) it is straightforward to extract the splitting probability shown in Eq. (48) since by construction $\tilde{\mathcal{F}}(a, \epsilon \rightarrow 0|x_0) = \tilde{\mathcal{F}}(a, \epsilon \rightarrow 0|b) = 1$. We have in fact that

$$\tilde{S}_{a,b}(\epsilon|x_0) = \frac{1}{v} - \tilde{\mathcal{G}}_a(b, \epsilon|x_0) \int_a^b dx \tilde{P}(x, \epsilon|b) - \tilde{\mathcal{G}}_b(a, \epsilon|x_0) \int_a^b dx \tilde{P}(x, \epsilon|a), \quad (\text{D5})$$

Acknowledgements

We thank Nitant Kenkre for his continuous support and uncountable discussions on the paper. SG acknowledges the support and warm hospitality of the University of Bristol. The work started as an activity under the Advanced Study Group ‘‘Statistical Physics and Anomalous Dynamics of Foraging’’ held in 2015 at the Max Planck Institute for the Physics of Complex Systems, Dresden. This work was supported in part by the Engineering and Physical Sciences Research Council (EPSRC) UK Grant No. EP/I013717/1.

References

- [1] L. Giuggioli and V. M. Kenkre, ‘‘Consequences of animal interactions on their dynamics: emergence of home ranges and territoriality,’’ *Mov. Ecol.*, vol. 2, 2014.
- [2] L. Kusmierz, S. N. Majumdar, S. Sabhapandit, and G. Schehr, ‘‘First order transition for the optimal search time of lévy flights with resetting,’’ *Phys. Rev. Lett.*, vol. 113, p. 220602, Nov 2014.
- [3] P. Visco, R. J. Allen, S. N. Majumdar, and M. R. Evans, ‘‘Switching and growth for microbial populations in catastrophic responsive environments,’’ *Biophysical Journal*, vol. 98, no. 7, pp. 1099 – 1108, 2010.
- [4] M. R. Evans and S. N. Majumdar, ‘‘Diffusion with stochastic resetting,’’ *Phys. Rev. Lett.*, vol. 106, p. 160601, Apr 2011.
- [5] M. R. Evans and S. N. Majumdar, ‘‘Diffusion with resetting in arbitrary spatial dimension,’’ *J. Phys. A: Math. Theor.*, vol. 47, no. 28, p. 285001, 2014.
- [6] M. R. Evans, S. N. Majumdar, and K. Mallick, ‘‘Optimal diffusive search: nonequilibrium resetting versus equilibrium dynamics,’’ *J. Phys. A: Math. Theor.*, vol. 46, no. 18, p. 185001, 2013.
- [7] H. Touchette, E. Van der Straeten, and W. Just, ‘‘Brownian motion with dry friction: Fokker–Planck approach,’’ *J. Phys. A: Math. Theor.*, vol. 43, no. 44, p. 445002, 2010.
- [8] M. Chase, K. Spendier, and V. M. Kenkre, ‘‘Analysis of confined random walkers with applications to processes occurring in molecular aggregates and immunological systems,’’ *J. Phys. Chem. B*, vol. 120, no. 12, pp. 3072–3080, 2016.

- [9] P. Holgate, “Random walk models for animal behavior,” in Pennsylvania State statistics - Statistical ecology: sampling and modeling biological populations and population dynamics (G. Patil, E. Pielou, and W. Walters, eds.), vol. 2, pp. 1–12, University Park, PA, USA: Pennsylvania State University Press, 1971.
- [10] A. Okubo, Diffusion and ecological problems: mathematical models, vol. 10 *Biomathematics*. Berlin, Germany: Springer Verlag, 1980.
- [11] A. Okubo and L. Gross, “Animal movements in home range,” in Diffusion and Ecological Problems: Modern Perspectives, pp. 238–267, Springer, 2001.
- [12] V. M. Kenkre, Z. Kalay, and P. E. Parris, “Extensions of effective-medium theory of transport in disordered systems,” Phys. Rev. E, vol. 79, p. 011114, Jan 2009.
- [13] H. Wolf, “Energy transfer in organic molecular crystals: a survey of experiments,” in Advances in atomic and molecular physics (D. Bates and I. Eastermann, eds.), vol. 3, pp. 119–142, Elsevier, 1968.
- [14] S. L. Lima and L. M. Dill, “Behavioral decisions made under the risk of predation: a review and prospectus,” Canadian journal of zoology, vol. 68, no. 4, pp. 619–640, 1990.
- [15] V. M. Kenkre, “The master equation approach: Coherence, energy transfer, annihilation, and relaxation,” in Exciton dynamics in molecular crystals and aggregates (G. Hoehler, ed.), pp. 1–109, Springer, 1982.
- [16] E. W. Montroll and R. B. Potts, “Effect of defects on lattice vibrations,” Phys. Rev., vol. 100, pp. 525–543, Oct 1955.
- [17] V. M. Kenkre, “Theory of exciton annihilation in molecular crystals,” Phys. Rev. B, vol. 22, pp. 2089–2098, 1980.
- [18] H. C. Wolf and H. Port, “Excitons in aromatic crystals: trap states, energy transfer and sensitized emission,” J. Lumin., vol. 12, pp. 33–46, 1976.
- [19] D. D. Smith, R. C. Powell, and A. H. Zewail, “Direct measurement of excitation transport in a highly disordered quasi-one-dimensional solid,” Chem. Phys. Lett., vol. 68, pp. 309–313, 1979.
- [20] H. C. Wolf, “Energy transfer in organic molecular crystals: a survey of experiments,” Adv. At. Mol. Phys., vol. 3, p. 119142, 1967.
- [21] R. C. Powell and Z. G. Soos, “Singlet exciton energy transfer in organic solids,” J. Lumin., vol. 11, pp. 1–45, 1975.
- [22] A. Fort, V. Ern, and V. Kenkre, “Theory of coherence effects in time-dependent delayed fluorescence. ii. application to two-and three-dimensional crystals,” Chemical physics, vol. 80, no. 3, pp. 205–211, 1983.
- [23] K. Spendier, S. Sugaya, and V. M. Kenkre, “Reaction-diffusion theory in the presence of an attractive harmonic potential,” Phys. Rev. E, vol. 88, p. 062142, 2013.
- [24] V. M. Kenkre and S. Sugaya, “Theory of the transmission of infection in the spread of epidemics: interacting random walkers with and without confinement,” University of New Mexico preprint, 2014.
- [25] M. R. Evans and S. N. Majumdar, “Diffusion with optimal resetting,” J. Phys. A: Math. Theor., vol. 44, no. 43, p. 435001, 2011.
- [26] V. Giorno, A. Nobile, and L. Ricciardi, “On the densities of certain bounded diffusion processes,” Ric. Mat., vol. 60, no. 1, pp. 89–124, 2011.
- [27] A. Okubo and S. A. Levin, Diffusion and ecological problems: modern perspectives. New York, USA: Springer Verlag, 2nd ed., 2001.
- [28] L. Giuggioli, G. Abramson, V. M. Kenkre, R. Parmenter, and T. L. Yates, “Theory of home range estimation from displacement measurements of animal populations,” J. Theor. Biol., vol. 240, pp. 126–135, 2006.
- [29] G. E. Uhlenbeck and L. S. Ornstein, “On the theory of the brownian motion,” Phys. Rev., vol. 36, no. 5, pp. 823–841, 1930.
- [30] S. N. Majumdar, S. Sabhapandit, and G. Schehr, “Random walk with random resetting to the maximum position,” Phys. Rev. E, vol. 92, p. 052126, Nov 2015.

- [31] S. Reuveni, “Optimal stochastic restart renders fluctuations in first passage times universal,” Phys. Rev. Lett., vol. 116, p. 170601, Apr 2016.
- [32] S. Eule and J. J. Metzger, “Non-equilibrium steady states of stochastic processes with intermittent resetting,” New Journal of Physics, vol. 18, no. 3, p. 033006, 2016.
- [33] A. Nagar and S. Gupta, “Diffusion in presence of stochastic resetting at power-law times,” Phys. Rev. E, vol. 93, p. 060102(R), 2016.
- [34] C. Christou and A. Schadschneider, “Diffusion with resetting in bounded domains,” J. Phys. A: Math. Theor., vol. 48, no. 28, p. 285003, 2015.
- [35] A. Pal, “Diffusion in a potential landscape with stochastic resetting,” Phys. Rev. E, vol. 91, p. 012113, Jan 2015.
- [36] D. Boyer and C. Solis-Salas, “Random walks with preferential relocations to places visited in the past and their application to biology,” Phys. Rev. Lett., vol. 112, p. 240601, 2014.
- [37] S. N. Majumdar, S. Sabhapandit, and G. Schehr, “Dynamical transition in the temporal relaxation of stochastic processes under resetting,” Phys. Rev. E, vol. 91, p. 052131, May 2015.
- [38] M. Montero and J. Villarroel, “Monotonic continuous-time random walks with drift and stochastic reset events,” Phys. Rev. E, vol. 87, p. 012116, Jan 2013.
- [39] V. Méndez and D. Campos, “Characterization of stationary states in random walks with stochastic resetting,” Phys. Rev. E, vol. 93, p. 022106, Feb 2016.
- [40] L. Kusmierz, S. N. Majumdar, S. Sabhapandit, and G. Schehr, “First order transition for the optimal search time of lévy flights with resetting,” Phys. Rev. Lett., vol. 113, p. 220602, Nov 2014.
- [41] D. Campos and V. Méndez, “Phase transitions in optimal search times: How random walkers should combine resetting and flight scales,” Phys. Rev. E, vol. 92, p. 062115, Dec 2015.
- [42] A. Pal, A. Kundu, and M. R. Evans, “Diffusion under time-dependent resetting,” J. Phys. A: Math. Theor., vol. 49, no. 22, p. 225001, 2016.
- [43] X. Durang, M. Henkel, and H. Park, “The statistical mechanics of the coagulationdiffusion process with a stochastic reset,” J. Phys. A: Math. Theor., vol. 47, no. 4, p. 045002, 2014.
- [44] S. Gupta, S. N. Majumdar, and G. Schehr, “Fluctuating interfaces subject to stochastic resetting,” Phys. Rev. Lett., vol. 112, p. 220601, Jun 2014.
- [45] S. Gupta and A. Nagar, “Resetting of fluctuating interfaces at power-law times,” J. Phys. A: Math. Theor., vol. 49, p. 445001, 2016.
- [46] É. Roldán, A. Lisica, D. Sánchez-Taltavull, and S. W. Grill, “Stochastic resetting in backtrack recovery by RNA polymerases,” Phys. Rev. E, vol. 93, p. 062411, 2016.
- [47] J. Fuchs, S. Goldt, and U. Seifert, “Stochastic thermodynamics of resetting,” EPL (Europhysics Letters), vol. 113, no. 6, p. 60009, 2016.
- [48] A. Pal and S. Reuveni, “First passage under restart,” Phys. Rev. Lett., vol. 118, p. 030603, Jan 2017.
- [49] M. R. Evans, S. N. Majumdar, and K. Mallick, “Optimal diffusive search: nonequilibrium resetting versus equilibrium dynamics,” Journal of Physics A Mathematical General, vol. 46, p. 185001, May 2013.
- [50] Ł. Kuśmierz, M. Bier, and E. Gudowska-Nowak, “Optimal potentials for diffusive search strategies,” Journal of Physics A Mathematical General, vol. 50, p. 185003, May 2017.
- [51] S. Belan, “Restart Could Optimize the Probability of Success in a Bernoulli Trial,” Physical Review Letters, vol. 120, p. 080601, Feb. 2018.
- [52] Ł. Kuśmierz and E. Gudowska-Nowak, “Optimal first-arrival times in Lévy flights with resetting,” Phys. Rev. E, vol. 92, p. 052127, Nov. 2015.
- [53] C. Christou and A. Schadschneider, “Diffusion with resetting in bounded domains,” Journal of Physics A Mathematical General, vol. 48, p. 285003, July 2015.
- [54] A. Chatterjee, C. Christou, and A. Schadschneider, “Diffusion with resetting inside a circle,” Phys. Rev. E, vol. 97, p. 062106, June 2018.
- [55] E. Roldán and S. Gupta, “Path-integral formalism for stochastic resetting: Exactly solved examples

- and shortcuts to confinement,” Phys. Rev. E, vol. 96, p. 022130, 2017.
- [56] O. Bénichou, Y. Kafri, M. Sheinman, and R. Voituriez, “Searching fast for a target on dna without falling to traps,” Phys. Rev. Lett., vol. 103, p. 138102, 2009.